 DOI: 10.1002/eji.202048941 Eur. J. Immunol. 2021. 51: 672–681

European Journal of Immunology

Allergy and inflammation

Short Communication

Deep phenotypical characterization of human CD3$^+$CD56$^+$ T cells by mass cytometry

Addi J. Romero-Olmedo[*1], *Axel R. Schulz*[*2], *Magdalena Huber*[1], *Corinna U. Brehm*[3,4], *Hyun-Dong Chang*[2], *Cristina M. Chiarolla*[5], *Tobias Bopp*[6], *Chrysanthi Skevaki*[7], *Friederike Berberich-Siebelt*[5], *Andreas Radbruch*[2], *Henrik E. Mei*[**2] and *Michael Lohoff*[**1]

[1] Institute for Medical Microbiology and Hospital Hygiene, University of Marburg, Marburg, Germany
[2] German Rheumatism Research Center Berlin (DRFZ), Leibniz Institute, Berlin, Germany
[3] Comprehensive Biobank Marburg – CBBMR, Member of the DZL, Philipps-University Marburg, Marburg, Germany
[4] Institute for Pathology, University Hospital Marburg, Philipps-University Marburg, Marburg, Germany
[5] Institute of Pathology, Julius-Maximilian University of Wuerzburg, Wuerzburg, Germany
[6] Institute for Immunology, University Medical Center of the Johannes Gutenberg-University Mainz, Mainz, Germany
[7] Institute of Laboratory Medicine, Universities of Giessen and Marburg Lung Center (UGMLC), Philipps University Marburg, German Center for Lung Research (DZL), Marburg, Germany

CD56$^+$ T cells are a group of pro-inflammatory CD3$^+$ lymphocytes with characteristics of natural killer cells, being involved in antimicrobial immune defense. Here, we performed deep phenotypic profiling of CD3$^+$CD56$^+$ cells in peripheral blood of normal human donors and individuals sensitized to birch-pollen or/and house dust mite by high-dimensional mass cytometry combined with manual and computational data analysis. A co-regulation between major conventional T-cell subsets and their respective CD3$^+$CD56$^+$ cell counterparts appeared restricted to CD8$^+$, MAIT, and TCRγδ$^+$ T-cell compartments. Interestingly, we find a co-regulation of several CD3$^+$CD56$^+$ cell subsets in allergic but not in healthy individuals. Moreover, using FlowSOM, we distinguished a variety of CD56$^+$ T-cell phenotypes demonstrating a hitherto underestimated heterogeneity among these cells. The novel CD3$^+$CD56$^+$ subset description comprises phenotypes superimposed with naive, memory, type 1, 2, and 17 differentiation stages, in part represented by a phenotypical continuum. Frequencies of two out of 19 CD3$^+$CD56$^+$ FlowSOM clusters were significantly diminished in allergic individuals, demonstrating less frequent presence of cells with cytolytic, presumably protective, capacity in these donors consistent with defective expansion or their recruitment to the affected tissue. Our results contribute to defining specific cell populations to be targeted during therapy for allergic conditions.

Keywords: allergy · CD56 · human · mass cytometry · T cells

Additional supporting information may be found online in the Supporting Information section at the end of the article.

Correspondence: Prof. Michael Lohoff
e-mail: lohoff@med.uni-marburg.de

*Both the authors contributed equally to this work.
**Both the authors jointly directed this work.

Introduction

CD56, or neural cell adhesion molecule (NCAM), is found on most natural killer (NK) cells and a subset of $CD3^+$ T cells making up between 1 and 11% of peripheral blood lymphocytes [1,2]. Nomenclature of $CD56^+$ T cells can be controversial; they are often referred to as NK-like T cells or $CD3^+CD56^+$ NKT-like cells [2–4]. $CD56^+$ T cells may also express other NK cell markers, and comprise $TCR\gamma\delta^+$ T cells as well as $CD4^+$, $CD8^+$, and $CD4^-CD8^-$ double-negative (DN) T cells expressing diverse or invariant (iNKT, CD1d-restricted) αβ chains of the TCR [4,5]. Moreover, a $CD56^+$ population among $TCRV\alpha7.2^+CD161^+$ mucosal associated invariant T (MAIT) cells has been described with increased responsiveness to cytokine stimuli [6]. CD56 expression on $CD3^+$ T cells has been associated with enhanced cytotoxicity and pro-inflammatory function [1]. Activated CD1d-restricted NKT cells produce a variety of cytokines and chemokines, making them players in host immune responses during several pathologies including allergy. For instance, $CD4^+$ NKT cells generate IL4 and IL13, crucial during Th2-driven allergic reactions. In the lung, Type-2 CD1d-restricted NKT cells are involved in allergen-induced airway hyperreactivity [7,8]. However, a systematic analysis of $CD56^+$ T cells aiming at a better understanding of their phenotypic and functional heterogeneity has not been performed so far.

Here, we have performed a deep phenotyping of human peripheral blood $CD56^+$ T cells by 41-parameter mass cytometry (MC). Due to the above-mentioned controversial nomenclature when describing $CD56^+$ or $CD57^+$ T cells with or without CD1d-restriction as "NKT" cells, we will refer to the herein studied cells as $CD3^+CD56^+$ to provide an accurate nomenclature of these cells instead of "NKT-like cells." We could distinguish 19 phenotypically distinct populations of $CD3^+CD56^+$ T cells including multiple innate-like and classical T-cell populations, indicating a hitherto underestimated heterogeneity among these cells. A systematically comparison of the frequencies and co-relatedness of $CD3^+CD56^+$ subsets in healthy donors and donors suffering from allergy to house dust mites (HDMs) or birch pollen (BP), the major airborn allergens and common inducers of allergic asthma, disclosed a dysregulated $CD3^+CD56^+$ T-cell compartment in the blood of allergic individuals.

Results and discussion

We used a panel of 41 antibodies (Supporting Information Table S1) to detect and comprehensively phenotype NK cells and T lymphocyte subsets, including $CD56^+$ T cells, in cryopreserved PBMC samples obtained from the blood of 14 allergic donor (AD) and 13 healthy donor (HD) volunteers (Supporting Information Table S2). For MC analysis, frozen PBMC were thawed, barcoded [9,10], and stained to reveal the expression of T cell, NK cell, and accessory markers. After data acquisition and de-barcoding, we manually gated $CD4^+$ T cells, $CD8^+$ T cells, $CD4^-CD8^-$ (DN) T cells, $TCR\gamma\delta^+$ T cells, MAIT cells, and $CD3^-CD56^+CD16^+$ NK cells from live, $CD45^+$ cells (Supporting Information Fig. S1A). As expected and consistent with their characteristic phenotype shown in the heat map, $CD4^+$, $CD8^+$, $TCR\gamma\delta^+$ T cells, and MAIT cells occupied designated areas of the t-SNE [11] map of live PBMCs (Fig. 1A and B). These cells were distinct from each other and from non-T/NK cells (DUMP), while DN T cells were scattered across the map and partly overlapped with areas of $CD8^+$, $TCR\gamma\delta^+$, MAIT, and non-T/NK cells (Fig. 1A and B). Additionally, we observed that $CD3^+CD56^+$ cells were present in all major $CD3^+$ T-cell subsets (Fig. 1A). Overall, $CD3^+$ cells comprised similar frequencies of $CD56^+$ cells in HD and AD (5.2% and 4.0%, median, $p = 0.55$, Mann–Whitney U-test). No significant correlations (Spearman) were identified between frequencies of $CD3^+CD56^+$ cells and the donors' age, gender, and amounts of specific (s)IgE in both groups. $CD3^+CD56^+$ T cells did not form a separate population in the t-SNE projection of total PBMCs, but constituted parts of areas occupied by $CD4^+$, $CD8^+$, $TCR\gamma\delta^+$, DN, and MAIT cells, respectively, suggesting that $CD3^+CD56^+$ cells largely share the phenotypical setup of their parent T-cell subset (Fig. 1A). Thus, we started exploring $CD3^+CD56^+$ T cells by manually gating $CD4^+$, $CD8^+$, DN, $TCR\gamma\delta^+$, and MAIT cell subsets among the $CD3^+CD56^+$ population (Supporting Information Fig. S1B). $CD3^+CD56^+$ T cells comprised mainly $CD8^+$ and $TCR\gamma\delta^+$ cells (median, 36.1% and 27.1%; AD and HD combined) as compared to lower abundant $CD4^+$, DN, and MAIT cells making up 6.4%, 9.0%, and 4.9%, respectively. We did not find significant differences in the distribution of these subsets between AD and HD (Fig. 1C), and no significant correlations with demographic and clinical data except an inverse correlation of the frequency of $CD3^+CD56^+$ DN T cells with age in HD (r, -0.64, $p = 0.027$), a trend not shown by AD ($r = 0.32$, $p = 0.28$, data not shown).

However, we did find correlations between the frequencies of total $CD8^+$, $TCR\gamma\delta^+$, and MAIT T cells and their corresponding daughter $CD3^+CD56^+$ T-cell subsets in both HD and AD groups. This was not true for total DN T versus DN $CD56^+$ T cells or $CD4^+$ T versus $CD4^+CD56^+$ T cells in both donors' cohorts. This finding indicates a co-regulation between particular T-cell subsets and their daughter CD56-expressing subsets (Fig. 1D). Furthermore, this co-regulation appears to be dictated by the T cell rather than the NK cell ontogeny, because we found no correlation between total NK cells and frequencies of the $CD3^+CD56^+$ subsets ($p > 0.12$, data not shown). Next, we were interested to see whether the different $CD56^+$ T-cell subsets are regulated together or independently and whether this is affected in allergic conditions. Therefore, we performed a correlation analysis within the different $CD3^+CD56^+$ subsets and tested for associations between them. A positive and significant correlation was observed between frequencies of DN $CD56^+$ T cells and those of $CD8^+CD56^+$ or $TCR\gamma\delta^+CD56^+$ T cells in both HD and AD. Likewise, frequencies of $CD8^+CD56^+$ T cells and of $TCR\gamma\delta^+CD56^+$ T cells correlated in a positive and significant manner in both donors' groups. However, and contrary to HD, we observed positive correlations between frequencies of $CD4^+CD56^+$ T cells and those of $CD8^+CD56^+$ or DN $CD56^+$ T cells exclusively in allergic individuals (Fig. 1E).

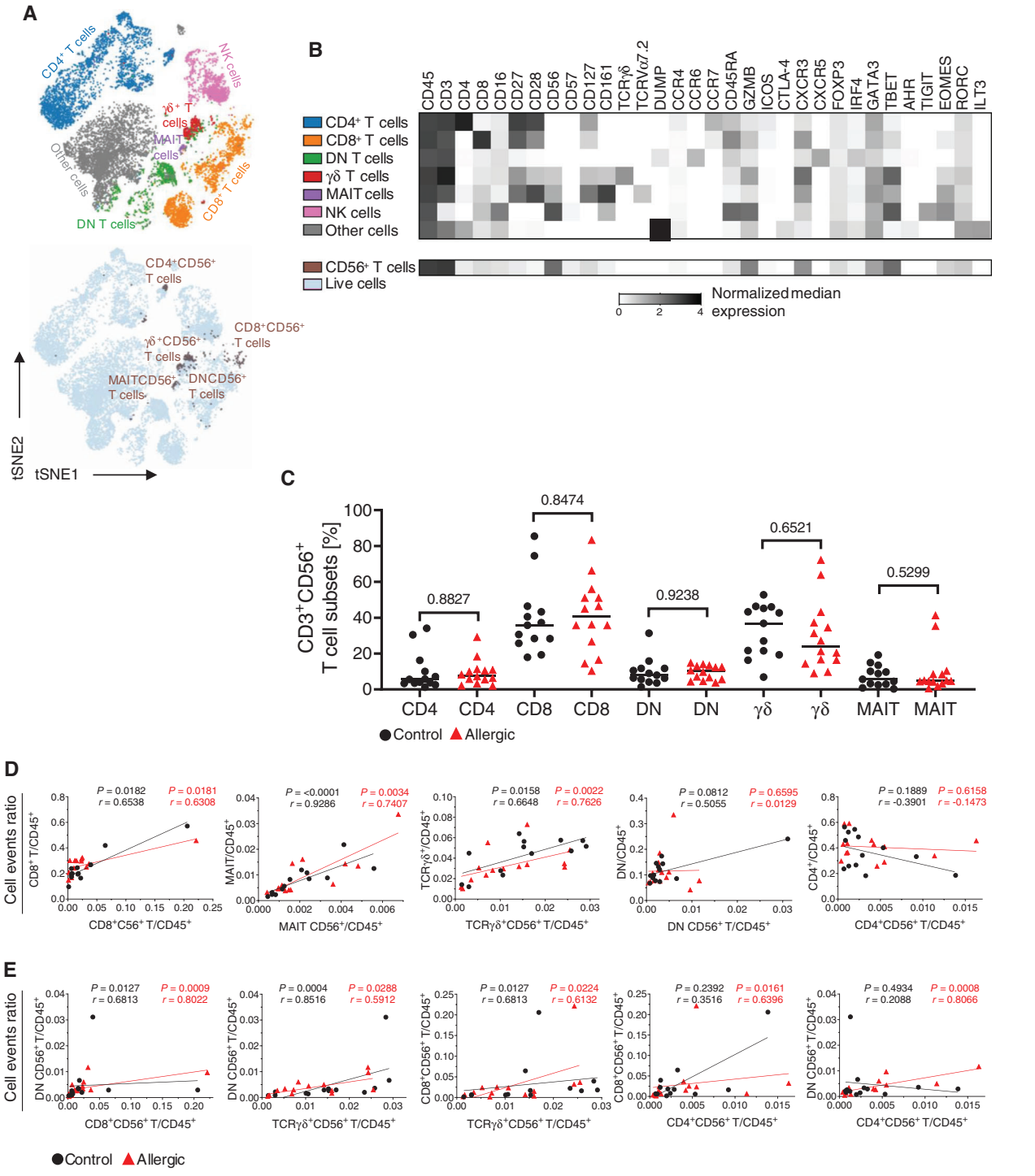

Figure 1. Differential emergence of CD56$^+$ cells within CD4$^+$, CD8$^+$, CD4$^-$CD8$^-$ (double negative, DN), γδ$^+$, and MAIT T cells in human blood. Human PBMCs were stained using a T-cell centric mass cytometry (MC) panel. (A) t-SNE visualization of MC data from PBMCs was used to identify manually gated natural killer (NK) cells and T-cell populations, colored as indicated (top). The same map (bottom) highlights T cells expressing CD56 as separated subpopulations of CD4$^+$, CD8$^+$, DN, γδ$^+$, and MAIT cells. (B) Heat map showing median arcsinh-transformed signal intensities of select markers (columns) within the indicated manually gated cell populations (rows). (A and B) Representative sample of total samples measured (control $n = 13$, allergic $n = 14$). (C) Comparisons of CD3$^+$CD56$^+$ cell frequencies within CD4$^+$, CD8$^+$, DN, γδ$^+$, and MAIT cells between control and allergic donors. Numbers indicate p-values (unpaired Student's t-test with Welch's correction). Horizontal lines indicate median values. (D) Results of the correlation analysis between the indicated frequencies of conventional T-cell subsets in live CD45$^+$ cells (y-axis) and the frequencies of the respective CD3$^+$CD56$^+$ cell subsets in CD45$^+$ cells (x-axis) of individual donors. (E) Results of correlation analysis between frequencies of the indicated CD3$^+$CD56$^+$ subsets among live CD45$^+$ cells of individual donors. (D and E) Spearman's correlation test. (C–E) Each dot represents one donor (controls $n = 13$, allergic $n = 14$). (A–E) Data were collected in one synoptic measurement of PBMCs from 27 donors (healthy $n = 13$, allergic $n = 14$).

This observation indicates an acquired co-dependency in the regulation of some $CD3^+CD56^+$ cell subsets that does not occur in normal individuals. There were no correlations between the frequencies of the remaining $CD3^+CD56^+$ cell subsets in AD or HD (Supporting Information Fig. 1C). Taken together, $CD3^+CD56^+$ cells are mainly composed of $CD8^+$ and $TCR\gamma\delta^+$ cells in healthy and allergic individuals. Moreover, the demonstrated correlation between specific $CD3^+CD56^+$ T-cell subsets only in allergic donors possibly relates to the immune pathophysiology of allergy involving cytokines such as IL-4 and IL-13 [7,8,12].

Next, we performed a systematic phenotypical characterization of the $CD3^+CD56^+$ T cells based on concatenated data from all 27 PBMC samples (Fig. 2A and Supporting Information Fig. S2A). $CD3^+CD56^+$ lymphocytes showed heterogeneous expression of several cell activation, differentiation, cytotoxicity, and exhaustion markers disclosing significant phenotypical heterogeneity (Fig. 2A) of $CD56^+$ T cells beyond the subsets described above (Fig. 2B). We detected differential expression of CD27, CD28, CD45RA, CD57, CD127, CD161, granzyme B (GZMB), TBET, CXCR3, EOMES, and TIGIT, and minor fractions of $CD3^+CD56^+$ T cells also expressed CCR7, CCR4, PD-1, or ICOS. This additional heterogeneity of $CD56^+$ T cells was neither restricted to nor redundant with known subfractions of $CD3^+CD56^+$ T cells, but was evident in $CD4^+$, $CD8^+$, DN, $TCR\gamma\delta^+$, and MAIT subsets (Fig. 2A and B).

To assess the size and characteristics of $CD3^+CD56^+$ T-cell subsets beyond the manually gated ones, and to fully consider the uncovered heterogeneity, we used FlowSOM clustering combined with hierarchical meta-clustering [13,14] to automatically distinguish 20 individual subsets (that is, clusters) of $CD3^+CD56^+$ cells (Fig. 2C and D). This approach recapitulates the five major $CD3^+CD56^+$ cell subsets described above, and identifies additional subsets within these (Fig. 2B and C). The 20 clusters comprised seven clusters within $CD8^+CD56^+$ T cells (#1-6, 11), four clusters among $CD4^+CD56^+$ (#17-20), four among $TCR\gamma\delta^+CD56^+$ (#7,9,12,16), and three within the DN $CD56^+$ T cells (#8,10,13). While differential expression of TBET, CXCR3, CD127, CD8, and EOMES was detectable, $TCRV\alpha7.2^+CD161^+$ "MAIT" cells (#14) were not further subdivided at the chosen level of meta-clustering. Based on the low but notable expression of at least one exclusion marker (DUMP), cluster 15 was not further considered (Fig. 2C and Supporting Information Fig. S2B). Clusters 1, 9, and 14 were the most abundant clusters representing at average 23%, 18%, and 11% of total $CD3^+CD56^+$ T cells, respectively. All other individual clusters represented between 0.05% and 7.3% of $CD3^+CD56^+$ T cells.

Among the clusters, two major families with high or low GZMB expression were identified, indicating the presence of $CD3^+CD56^+$ cell subsets with different cytotoxic potential. Interestingly, the clusters (except #4, 10) in the GZMB high-expressing family show increased median TBET expression. Moreover, all clusters in this family lacked CD4, CD25, CD28, CCR7, $TCRV\alpha7.2$, and PD-1. In terms of hierarchy, the more-cytotoxic family has two ramifications; the major difference between them lies in whether or not their cells express $TCR\gamma\delta$. Cells in the $TCR\gamma\delta^-$ (presumably $TCR\alpha\beta^+$) clusters show moderate TIGIT expression and comprise cluster 2 (single subgroup) and seven other clusters (#1, 3–6, 8, 10) that form a second group. Cluster 2 expresses the highest average levels of GZMB (among all 19 clusters) and contains $CD8^+$ cells with variable IRF4, CXCR3, CD57, and CD45RA expression. Collectively, cluster 2 represents a population with high cytotoxic potential (Fig. 2A and D). The other $TCR\gamma\delta^-$ clusters display differential EOMES expression and, interestingly, CD16 staining was dominant over CD8 in the hierarchical arrangement of these clusters. For instance, clusters 1, 3, 4, 8, 10 exhibit less CD16 expression than clusters 5 and 6. The distinctive features of cluster 3 are increased expression of TIGIT and EOMES in the presence of CD27, which points toward less differentiated cells. Due to the high expression of CD8, CD16, CD57, and GZMB, we consider clusters 5 and particularly 6 as containing activated cytotoxic T lymphocytes (CTLs). Previously, CTLs co-expressing CD57 and GZMB have also been described in myocardial infarction and chronic graft-versus-host disease [15,16]. The second group of more cytotoxic cells includes the $TCR\gamma\delta$-expressing clusters 16, 9, and 7. Clusters 16 and 9, but not cluster 7, contain mainly $CD27^+$, $CD127^+$, and $CD161^+$ cells indicating a combined cytotoxic potential and IFN imprint [1,12]. Cluster 7 displays high expression of CD45RA and co-expression of CD57, TIGIT, and CD8, conferring an unconventional phenotype similar to cells responding to IL-2 and expressing the cytotoxic mediators IFN-γ and TNF-α [17].

Strikingly, all clusters from the less-cytotoxic family, except 18, contain cells expressing moderate to high levels of CD28 and lack CD57, a feature clearly in contrast to all more cytotoxic clusters. Another remarkable contrast is the presence of CD127-expressing cells in all clusters of the less cytotoxic compared to the more cytotoxic family. The less cytotoxic family involves two major families, each with two further subdivisions. Clusters 11–14 form a group that is characterized by average levels of $CD27^+$, $CXCR3^+$, $EOMES^+$, and $TBET^+$ cells. Cells in cluster 11 express CD8 but lack CCR4, CD25, and CD161 reflecting, together with the other $CD8^+$ clusters, the paucity of Tc2 and Tc17 phenotypes or cells responding to IL-2. Our observations on cluster 14, including reduced PD-1 expression, are in line and complement what has been reported about CD56-expressing MAIT cells, which also represent a subset with increased IFN-γ response [6]. Beyond differential expression of $TCR\gamma\delta$, CD4/CD8, and $TCRV\alpha7.2$, clusters 12–14 are very similar; interestingly, a fraction of cluster 14 also contains $CD8^+$ cells. Although clusters 17–20 shared CD4 expression, they are placed in two different groups. This can be explained by their differentiation status [18] since clusters 17 and 20 showed CD45RA and CCR7 expression, which was absent in clusters 18 and 19. Cells in cluster 17 were the only ones expressing CCR4, ICOS, CTLA-4, CCR10, CRTH-2, and also co-expressed CD16 and CD28, collectively indicating a Th2 phenotype. However, some cluster 17 cells also expressed FOXP3, yet in the absence of CD25. The phenotype of cluster 20 indicates a naive phenotype with high expression of CD27, CD45RA, CCR7, and CD16. Cluster 19 cells are characterized by CD161, CXCR3, and CD127 expression, similar to Th17 cells.

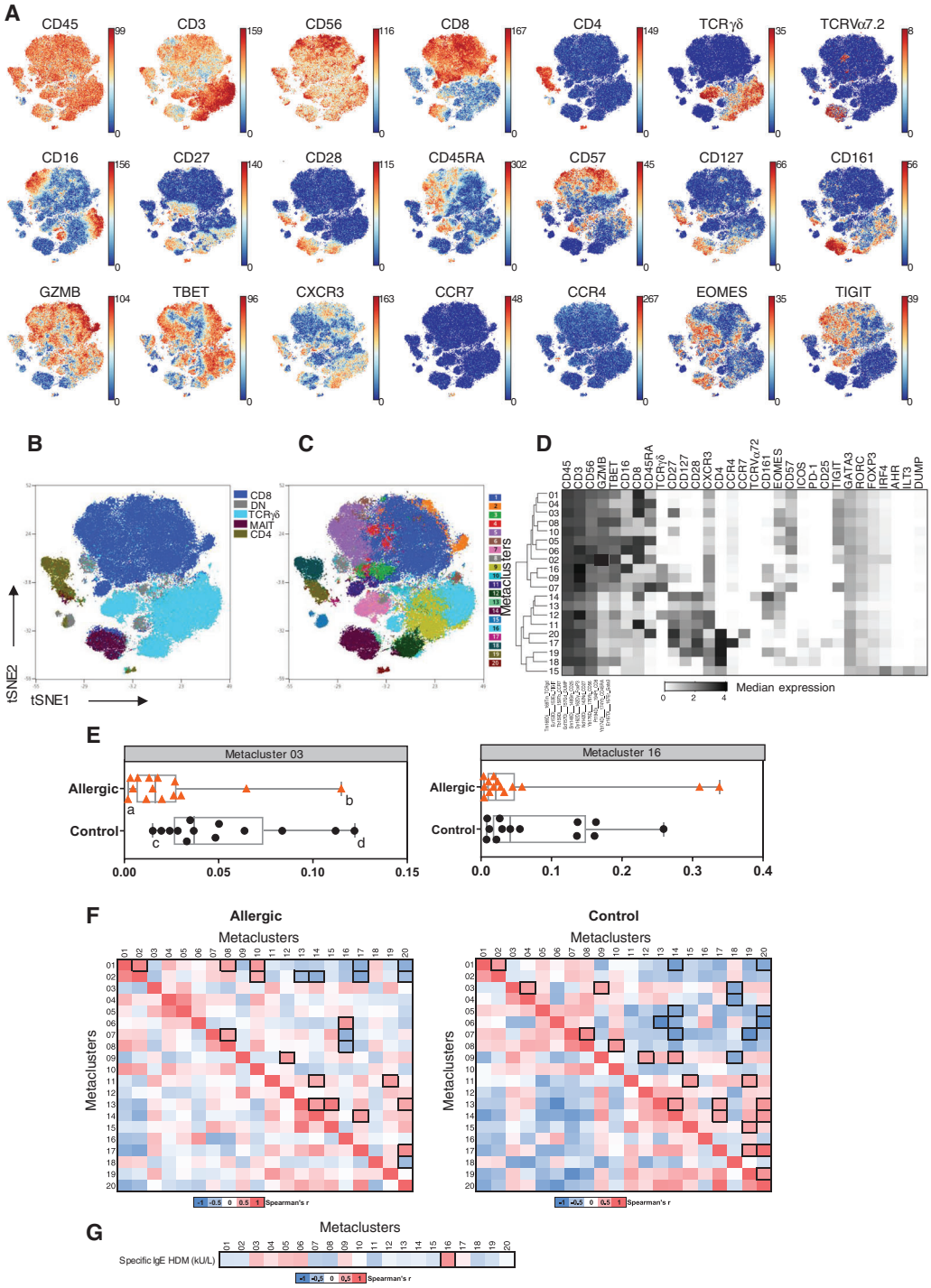

Figure 2. Characterization and clustering of $CD3^+CD56^+$ cell subsets. (A) Mass cytometry data from PBMCs of 27 donors were concatenated and depicted as two-dimensional t-SNE maps showing expression levels (dark red color, high expression; dark blue color, no expression) of selected markers. All markers shown in Supporing Information Table S1 were used to calculate t-SNE coordinates. (B) t-SNE plot as in Fig. 2A, depicting the distribution of the five manually gated $CD3^+CD56^+$ cell subsets. (C) t-SNE plot as in Fig. 2A, depicting 20 cell clusters after FlowSOM clustering and subsequent meta-clustering. Numbers within colored boxes correspond to the respective cluster number. (D) Heat map visualizing the phenotype of the 20 $CD3^+CD56^+$ cell clusters, each cluster contains concatenated data of the 27 donors. (E) Results from the significance analysis of microarrays (SAM) performed in OMIQ (www.omiq.ai). The boxplots show the abundance of the clusters with a significant difference between control ($n = 13$) and allergic ($n = 14$) individuals. Data points (solid dots/triangles) represent donors, lower and upper quartiles (left and right end of boxes, respectively), median values (lines within the boxes), and range of data from minimum to maximum (whiskers). (F) Correlations between cluster frequencies in allergic individuals and healthy controls. (G) Correlations between cluster frequencies and HDM-specific IgE titers. (F and G) Spearman's correlation test; boxed fields indicate p-values of less than 0.05 for the correlation. (A–G) Data were collected (as in Fig. 1) in one synoptic measurement of PBMCs from (A–F) 27 donors (healthy $n = 13$, allergic $n = 14$) and (G) only allergic ($n = 13$).

Cluster 18 comprised $CCR7^-CD45RA^-CD28^-CD27^-$ differentiated cells, with expression of CXCR3, PD-1, CD127 but not TIGIT, low EOMES and the highest CD57, GZMB, and CD56 signal among the less cytotoxic family. Median staining intensities for LAG3, AHR, NKp46, NKp44, CCR6, ILT3, TIM3, and IRF1 were homogeneous and mostly low, and did not reveal differential expression between the 19 $CD3^+CD56^+$ cell clusters.

Together with their very low to no staining for CD27 (except clusters 3, 9, and 10), CD28, and CD127, but CD45RA expression, the family of more cytotoxic $CD3^+CD56^+$ cell clusters share characteristics with late differentiated cells [1,18–20]. On the other hand, less cytotoxic $CD3^+CD56^+$ clusters (except cluster 20) show very little or no presence of $CD45RA^+$ cells, displaying an effector memory and intermediate/advanced differentiated phenotype, which also includes CD27, CD127, and CD28 expression [18,19]. Based on little or no expression of CCR7, we observed a strong predominance of effector phenotypes in all clusters, except for cluster 20. These results enrich and are in line with other reports [3,4]. One of the properties of NK cells and CTLs is the release of GZMB, the strongest human granzyme produced by CTLs [21]. Additionally, in $CD8^+$ T cells, GZMB expression has been associated with the progress of differentiation defined by CCR7, CD27, and CD45RA [19]. In line with the reported associations between CD27, CD28, CD127, CD161, CCR7, CD45RA, TBET, and GZMB in conventional T cells [19,21–29], our results demonstrate a direct inverse association between $GZMB^+$ cells and $CD27^+$, $CD28^+$, $CD127^+$, and $CD161^+$ also in $CD3^+CD56^+$ cells, perhaps indicative of the grade of differentiation [30]. Considering CD45RA expression in addition, their phenotype is in fact very similar to effector memory T cells re-expressing CD45RA (TEMRA) [30–33].

The t-SNE map (Fig. 2A, Supporting Information Fig. S2B) suggests that some clusters belong to a phenotypical continuum, as indicated by the lack of clear cluster boundaries as seen for other clusters. For instance, clusters 1, 4, 5, and 6 are hardly separated in the population of $CD8^+CD3^+CD56^+$ cells, while $CD8^+$ clusters 2 and 3 appear to have more distinct locations on the map. Similarly, clusters 9 and 16 also appear to contribute one greater population of $TCR\gamma\delta^+CD3^+CD56^+$ cells. For most other subsets, there is a good agreement between the grouping of cells by t-SNE and the results of FlowSOM clustering. Interestingly, these observations are in agreement with and confirm the unsupervised hierarchical arrangement of the clusters (Fig. 2B). On the other hand, some cells clustered together still show heterogeneity (such as cluster 14), suggesting that some clusters comprise additional subsets that were not fractionated using a target metacluster count of 20. Together, these data indicate that $CD3^+CD56^+$ T cells are more heterogeneous than previously appreciated; they comprise $CD56^+$ T-cell populations that phenotypically resemble type 1, 2, 17, and MAIT cells. Apparently, all major known $CD3^+CD56^+$ T cells lineage can acquire a cytotoxic phenotype, indicating compatibility of the transcriptional programs conferring cytotoxicity and polarization.

Next, we employed significance analysis of microarrays to systematically identify clusters with differential abundance in HD versus AD. This analysis revealed reduced proportions of clusters 3, 6, 11, and 16 in allergic individuals. In particular, cluster 3 was remarkably less abundant in AD than in HD (Fig. 2E), while the differences in clusters 6 and 11 appear related to outliers (Supporting Information Fig. S3A). In line with a cytotoxic/Tc1 phenotype [34], cluster 3 was characterized by TBET, TIGIT, CD27, CD45RA, CXCR3, EOMES, CD16, and CD57 expression (Fig. 2D). We selected four donors (marked by a-d in Fig. 2E) and confirmed the differential abundance of cluster 3 cells by manual gating, in line with low or high CD27 expression (Supporting Information Fig. S3B). The fact that the frequencies of clusters 3 and 16 were consistently reduced in peripheral blood of allergic compared to control individuals (Fig. 2E), suggests that these cells might have activities protecting from allergy, and are either less expanded under allergic conditions, or have been recruited to the affected tissue. While our present results cannot differentiate between these possibilities, follow-up projects will seek to validate the present findings and to elucidate the role of specially $CD3^+CD56^+$ cluster 3 in immune homeostasis and allergy. Altogether, our findings may complement mechanisms of allergy described before [12].

We next addressed the co-regulation of the individual clusters by systematically performing Spearman correlations between all cluster frequencies found in HD and AD. We found more significant correlations (11 negative, 18 positive) between clusters from HD than from AD (7 negative, 14 positive). Interestingly, we observed a positive correlation between cluster 3 and the related clusters 4 (r, 0.65, $p = 0.0194$) (both $CD8^+$) and 9 (r, 0.62, $p = 0.0267$) (both $CD27^+$) and a negative correlation to cluster 18 (r, -0.57, $p = 0.0448$) only in HD, while no such correlations were observed for cluster 3 of AD (Fig. 2F), re-emphasizing the disturbed architecture of the $CD3^+CD56^+$ cell compartment in allergy. Finally, we analyzed whether frequencies of $CD3^+CD56^+$ T-cell clusters are associated with clinical and laboratory correlates of allergy. We observed a positive correlation between cluster 16 frequencies and HDM-specific IgE concentrations (r, 0.72, $p = 0.0047$) (Fig. 2G), despite the high cytotoxic and low type 2-like activity of this cluster. In view of the overall reduced frequencies of cluster 16 in allergy, the correlation with allergen-specific plasma IgE can presently not be rationalized, while cluster 16 definitely deserves attention in follow-up studies. Furthermore, there were negative correlations between BP-specific plasma IgE concentrations and clusters 17 and 19, although this analysis was of very limited power as only 5 out of 14 individuals were sensitized to BP (data not shown).

Concluding remarks

In summary, our study provides a detailed characterization of $CD3^+CD56^+$ T cells in human blood by high-dimensional MC. By identifying the presence of $CD3^+CD56^+$ cells with different cytotoxic potential and phenotypes reminiscent of naive, effector memory, and type 1, 2 and 17 T cells, we here disclose a remarkable heterogeneity of $CD56^+$ cytotoxic T cells exceeding

the canonical subsetting into $CD4^+$, $CD8^+$, DN, $TCR\gamma\delta^+$, and MAIT type cells. Consistent with the disturbance of the overall architecture of $CD56^+$ T cells in allergy, we here identified $CD3^+CD56^+$ cell candidate populations that were significantly diminished under conditions of allergy. These data lay the foundation for exploring subsets of $CD56^+$ T cells as targets for allergy treatments.

Materials and methods

Donor sample preparation for MC and specific IgE determination

Adult individuals were invited to participate in our study after approval from the ethics committee of the medical faculty of the Phillipps-University Marburg (study number 19/17-08042018). Participants were recruited on March 6, 2019, showing rhinoconjunctivitis or stating to be free of any seasonal allergy. After written informed consent was obtained, blood from 27 volunteers was collected on the same day by phlebotomy using mononuclear cell preparation tubes (CPT™, BD Vacutainer), and PBMCs were isolated as per manufacturer's instructions. Then PBMCs were washed once in 15 mL PBS (diluted with MilliQ water from 10x PBS, Rockland) and centrifuged at 300 x *g* for 5 min at 4°C in a refrigerated centrifuge (4-16K; Sigma Aldrich). PBMCs were washed again as before and the cell pellet was re-suspended in Cryostor™ CS10 cryopreservation media (BioLife Solutions) at $\sim 4\times10^6$ cells/mL. Cryovials were then transferred to a −80°C freezer overnight. Cryopreserved samples were then transferred to the gas phase in a liquid nitrogen tank for storage. Sensitization to birch-pollen and HDM was confirmed by measuring specific IgE levels in plasma against Dermatophagoides pteronyssinus extract and against Betula verrucosa extract, respectively, using the immunoCAP assay (Thermo Fisher Scientific) according to the manufacturer's instructions.

Antibodies and reagents for MC

Antibodies (Supporting Information Table S1) were obtained preconjugated to metal isotopes (Fluidigm) or in purified form from Biolegend, Miltenyi Biotec, BD Biosciences, Thermo Fisher Scientific, R&D Systems, Sanquin, or were produced in-house (DRFZ), and conjugated in-house using the MaxPar X8 kit (Fluidigm) following the manufacturer's instructions. Metal isotopes/elements not available from Fluidigm were purchased from Trace Sciences or Sigma-Aldrich. Isotopically enriched cisplatin was purchased from or kindly provided by Fluidigm. Palladium and cisplatin antibody conjugations were performed in-house as described before [9,35]. Fluorochrome-conjugated antibodies were purchased from Miltenyi Biotec and Cell Signaling Technologies. Fc blocking reagent was purchased from Miltenyi Biotec. All antibody mastermixes were cryopreserved at −80°C as described before [36]. Prior to use, thawed antibody mastermixes were centrifuged (4°C, 15 000 x *g*, 10 min) to remove potential aggregates. mDOTA-^{103}Rh, used for discrimination of dead cells, was prepared from DOTA-maleimide (Macrocyclics, Dallas, TX) and rhodium chloride (Sigma-Aldrich) as previously described [37] and stored at 4°C.

Cell staining and MC acquisition

On the day of the experiment, cryopreserved PMBCs from 27 samples ($\sim 4\times10^6$ cells/sample) (plus one anchor control for confirming staining stability of our antibody cocktail) were thawed in prewarmed (37°C) complete RPMI (Sigma-Aldrich; RPMI 1640, 10% FCS, glutamine, penicillin, and streptomycin) supplemented with 2.5 U/mL Benzonase HC (Millipore), and centrifuged (4°C, 500 x *g*, 5 min). Afterwards, each cell pellet was re-suspended in 3 mL CyTOF staining medium (1x PBS (prepared from 10x PBS (Rockland Immunochemicals), 0.5% (w/v) BSA (PAN-Biotech), and 0.02% sodium azide (Sigma-Aldrich)) containing 0.5 U/mL Benzonase HC (CSM+B). Cells were filtered through a 30 μm cell strainer and 2×10^6 cells per sample were used in the subsequent barcode staining [9,10]. Cryopreserved barcode antibody mixes containing combinations of metal-conjugated ^{89}Y-, ^{104}Pd-, ^{106}Pd-, ^{108}Pd-, ^{110}Pd-, ^{195}Pt-, ^{196}Pt-, and ^{198}Pd-labeled β-2-microglobulin (B2M) antibodies [9] were generated using an 8-choose-2 barcoding scheme. Barcode staining mixes were supplemented with 1 μL Fc blocking solution (Miltenyi Biotec), and CD19-, CD20-, CD36-, and CD123-PE conjugates. On the day of the experiment, barcode mastermixes were thawed and used to stain individual cell samples in 50 μL for 30 min at 4°C in 250 μL PCR tubes. Subsequently, barcoded cells were transferred to a 2 mL V-bottom deep well plate (Corning), and washed four times with 1.2 mL CSM+B. Then, all samples were pooled into a 15-mL centrifuge tube (Sarstedt), washed twice in CSM+B, and transferred to a 5 mL Falcon® tube (Corning), where cells were re-suspended in 400 μL previously cryopreserved antibody cocktail [36] to stain cell-surface markers (Supporting Information Table 1). Cells were incubated for 30 min at 4°C and washed once in 3 mL 1 x PBS, and then incubated at room temperature (RT) for 5 min in 1 mL PBS containing 2 μL ^{103}Rh-mDOTA to label dead cells, and then washed once in 3 mL CSM. Then, cells were resuspended in 1 mL fixation/permeabilization solution prepared from the FoxP3 Staining Buffer Set (Miltenyi Biotec) according to manufacturer's instructions and incubated for 45 min at 4°C, washed once with 3 mL CSM (700 x *g*, 5 min, 4°C), re-suspended in 1 mL 1 x permeabilization buffer prepared from the FoxP3 Staining Buffer Set (Miltenyi Biotec), incubated for 10 min at RT, and centrifuged (700 x *g*, 5 min, 4°C). Next, cells were stained with a cocktail of antibodies directed against intracellular markers (Supporting Information Table S1) in 400 μL 1 x permeabilization buffer, and incubated for 30 min at RT. Cells were then washed twice with 2 mL 1 x permeabilization buffer, re-suspended in 400 μL permeabilization buffer containing 4 μL ^{172}Yb-labeled anti-Cy5 antibody, and incubated for 30 min at RT. Subsequently, cells were

washed twice with 2 mL 1 x permeabilization buffer and incubated at 4°C for overnight in 2 % paraformaldehyde solution (diluted from 16% stock solution, Electron Microscopy Sciences in 1 x PBS). On the next day, cells were washed once in 1 mL CSM (700 x *g*, 5 min, 4°C) and then incubated 25 min, RT in 1 mL 1 x PBS supplemented with 1/ 500 v/ v 0.125 mM iridium-based DNA intercalator (Fluidigm). Cells were then washed once with 3 mL CSM and with 3 mL 1 x PBS and counted on a MACSQuant flow cytometer (Miltenyi Biotec). The sample pool was washed twice with 3 mL Millipore water and pelleted by centrifugation at 800 x g, 5 min, 4°C. Finally, cells were resuspended in an appropriate volume of water to a maximum of 7.5×10^5 cells/mL, filtered through a 35 μm cell strainer, supplemented with EQ Four Element beads (1/10, v/v) (Fluidigm), and acquired at an injection rate of 30 μL/min on a Helios mass cytometer (Fluidigm) that was prepared for acquisition by tuning and cleaning according to the manufacturer's advice, using tuning and cleaning solutions (Fluidigm) on the day of the measurement. The mass cytometer was run in dual calibration mode, with noise reduction turned on and event length thresholds set to 10 and 75.

MC data analysis

Raw MC data were converted to Flow Cytometry Standard (FCS) 3.0 files during acquisition. Data were normalized based on EQ Calibration Bead signals using CyTOF 6.7 software (Fluidigm). Next, data were compensated using the Catalyst algorithm [38] based on a spill-over matrix generated before [39]. Data were manually debarcoded using FlowJo (version 10.6.1) (FlowJo LLC, Ashland, OR) as described before [9]. From each of the resulting individual samples, single, live, CD45+ PBMCs were gated in FlowJo according to ^{103}Rh-mDOTA for dead cell exclusion, DNA and event length parameters, and CD45 expression (Supporting Information Fig. S1), and finally imported into and analyzed using OMIQ.ai (Santa Clara, CA) and Cytobank Premium (www.cytobank.org) data analysis platforms. FlowSOM [13] clustering and subsequent meta-clustering were performed in OMIQ (www.omiq.ai). Data visualizations, t-SNE plots [40], significance analysis of microarrays analysis, and heat-maps were generated in Cytobank [41], OMIQ [42], R studio, and Prism software. t-SNE coordinates were calculated using opt-SNE [42]. Pearson correlation test and Spearman's rank correlation analysis (two-tailed, 95% confidence interval) were employed. Data plotting and statistical analysis were performed using GraphPad Prism version 8.1.1.

Acknowledgements: This work was generously supported by the Else Kröner-Fresenius-Stiftung (Research group: "Functional, therapy-aimed clustering of T-cell sub-phenotypes across plasticity"). The authors thank Heike Hirseland for technical assistance, Dr. Sabine Baumgart for mass cytometry support, and Felix S.R. Picard and Dr. Hartmann Raifer for helpful discussions. Samples were pre-analytically processed and stored in Marburg Biobank CBBMR. ML is also supported by the Deutsche Forschungsgemeinschaft (DFG) (LO 396/8-1). CS is supported by the Universities Giessen and Marburg Lung Center (UGMLC), the German Center for Lung Research (DZL), University Hospital Giessen and Marburg (UKGM) research funding according to article 2, section 3 cooperation agreement, and the Deutsche Forschungsgemeinschaft (DFG)-funded SFB 1021 (C04), KFO 309 (P10), and SK 317/1-1 (Project number 428518790).
Open access funding enabled and organized by Projekt DEAL.

Author contributions: The study was designed and analyses were guided by M.L. with the input of H.E.M. M.H. and C.U.B. recruited the donors and organized the sampling. C.U.B. collected the blood samples. Mass cytometry was conducted by A.J.R.O., C.M.C., and A.R.S. at the DRFZ Berlin. C.S. performed sIgE tests. A.J.R.O., A.R.S., and H.E.M. analyzed data and made the figures. A.J.R.O., H.E.M., and M.L. drafted the manuscript. T.B. and F.B.S. supervised preliminary experiments and reviewed the manuscript. H.E.M., A.R.S., A.R., and H.D.C. reviewed and edited the manuscript.

Peer review: The peer review history for this article is available at https://publons.com/publon/10.1002/eji.202048941.

Data availability statement: The data that support the findings of this study are available in https://flowrepository.org at https://flowrepository.org/id/FR-FCM-Z34X, reference number FR-FCM-Z34X.

Conflict of interest: For C.S.: Consultancy and research funding, Hycor Biomedical, Bencard Allergie, and Thermo Fisher Scientific; Research Funding, Mead Johnson Nutrition (MJN). All other authors declare no commercial or financial conflict of interest.

References

1 **Van Acker, H. H., Capsomidis, A., Smits, E. L. and Van Tendeloo, V. F.**, CD56 in the immune system: more than a marker for cytotoxicity? *Front. Immunol.* 2017. **8**: 892.

2 **Almehmadi, M., Flanagan, B. F., Khan, N., Alomar, S. and Christmas, S. E.**, Increased numbers and functional activity of CD56+ T cells in healthy cytomegalovirus positive subjects. *Immunology* 2014. **142**: 258–268.

3 **Peng, L., Mao, F., Zhao, Y., Wang, T., Chen, N., Zhang, J., Cheng, P. et al.**, Altered phenotypic and functional characteristics of CD3+CD56+ NKT-like cells in human gastric cancer. *Oncotarget* 2016. **34**: 55222–55230.

4 **Montoya, C. J., Pollar, D., Martinson, J., Kumari, K., Wasserfall, C., Mulder, C., Rugeles, M. T. et al.**, Characterization of human invariant natural killer T subsets in health and disease using a novel invariant natural killer T cell-clonotypic monoclonal antibody, 6B11. *Immunology* 2007. **122**: 1–14.

5 **Norris, S., Doherty, D. G., Collins, C., McEntee, G., Traynor, O., Hegarty, J. E., and O'Farrelly, C.**, Natural T cells in the human liver: cytotoxic lymphocytes with dual T cell function are phenotypically heterogeneous and

include Vα24-JαQ and γδ T cell receptor bearing cells. *Hum. Immunol.* 1999. **60**: 20–31.

6 **Dias, J., Leeansyah, E., and Sandberg, J. K.**, Multiple layers of heterogeneity and subset diversity in human MAIT cell responses to distinct microorganisms and to innate cytokines. *Proc. Natl. Acad. Sci. USA* 2017. **114**: E5434–E5443.

7 **Slauenwhite, D., and Johnston, B.**, Regulation of NKT cell localization in homeostasis and infection. *Front. Immunol.* 2015. **6**: 255.

8 **Akbari, O., Stock, P., Meyer, E., Kronenber, M., Sidobre, S., Nakayama, T., Taniguchi, M. et al.**, Essential role of NKT cells producing IL-4 and IL-3 in the development of allergen-induced airway hyperreactivity. *Nat. Med.* 2003. **9**: 582–588.

9 **Schulz, A. R., and Mei, H. E.**, Surface barcoding of live PBMC for multiplexed mass cytometry. *Methods Mol. Biol.* 2019. **1989**: 93–108.

10 **Mei, H. E., Leipold, M. D., Schulz, A. R., Chester, C. and Maecker, H. T.**, Barcoding of live human PBMC for multiplexed mass cytometry. *J. Immunol.* 2015. **194**: 2022–2031.

11 **Maaten, L. V. D., and Hinton, G.**, Visualizing data using t-SNE. *J. Mach. Learn.* 2008. **9**: 2579–2605.

12 **Edwards, M. R., Strong, K., Cameron, A., Walton, R. P., Jackson, D. J., and Johnston, S. L.**, Viral infections in allergy and immunology: how allergic inflammation influences viral infections and illness. *J. Allergy Clin. Immunol.* 2017. **140**: 909–920.

13 **Van Gassen, S., Callebaut, B., Van Helden, M. J., Lambrecht, B. N., Demeester, P., Dhaene, T., and Saeys, Y.**, FlowSOM: using self-organizing maps for visualization and interpretation of mass cytometry data. *Cytometry A* 2015. **87**: 636–645.

14 **Nowicka, M., Krieg, C., Crowell, H. L., Weber, L. M., Hartmann, F. J., Guglietta, S., Becher, B. et al.**, CyTOF workflow: differential discovery in high-throughput high-dimensional cytometry datasets. *F1000Res*. 2017. **6**: 748.

15 **Stikvoort, A., Chen, Y., Rådestad, E., Törlén, J., Lakshmikanth, T., Björklund, A., Mikes, J. et al.**, Combining flow and mass cytometry in the search for biomarkers in chronic graft-versus-host disease. *Front. Immunol.* 2017. **8**: 717.

16 **Yu, H. T., Youn, J., Lee, J., Park, S., Chi, H., Lee, J., Choi, C. et al.**, Characterization of CD8+CD57+ T cells in patients with acute myocardial infarction. *Cell. Mol. Immunol.* 2015. **12**: 466–473.

17 **Kadivar, M., Petersson, J., Svensson, L., and Marsal, J.**, CD8αβ+ γδ T cells: a novel T cell subset with a potential role in inflammatory bowel disease. *J. Immunol.* 2016. **197**: 4584–4592.

18 **Kared, H., Martelli, S., Ng, T. P., Pender, S. L. F., and Larbi, A.**, CD57 in human natural killer cells and T-lymphocytes. *Cancer Immunol. Immunother.* 2016. **65**: 441–452.

19 **Bengsch, B., Ohtani, T., Herati, R. S., Bovenschen, N., Chang, K. and Wherry, E. J.**, Deep immune profiling by mass cytometry links human T and NK cell differentiation and cytotoxic molecule expression patterns. *J. Immunol. Methods* 2018. **453**: 3–10.

20 **Yang, Z., Kim, H. J., Villasboas, J. C., Price-Troska, T., Shahrzad, J., Wu, H., Luchtel, R. A. et al.**, Mass cytometry analysis reveals that specific intratumoral CD4+ T cell subsets correlate with patient survival in follicular lymphoma. *Cell. Rep.* 2019. **26**: 2178–2193.

21 **Hlongwane, P., Mungra, N., Madheswaran, S., Akinrinmade, O. A., Chetty, S., and Barth, S.**, Human granzyme B based targeted cytolytic fusion proteins. *Biomedicines*. 2018. **6**: 72.

22 **Fergusson, J. R., Fleming, V. M., and Klenerman, P.**, CD161-expressing human T cells. *Front. Immunol.* 2011. **2**: 36.

23 **Billerbeck, E., Kang, Y., Walker, L., Lockstone, H., Grafmueller, S., Fleming, V., Flint, J. et al.**, Analysis of CD161 expression on human CD8+ T cells defines a distinct functional subset with tissue-homing properties. *Proc. Natl. Acad. Sci. USA* 2010. **107**: 3006–3011.

24 **Northfiel, J. W., Kasprowicz, V., Lucas, M., Kersting, N., Bengsch, B., Kim, A., Phillips, R. E. et al.**, CD161 expressing on hepatitis C virus-specific CD8+ T cells suggest a distinct pathway of T cell differentiation. *Hepatology* 2008. **47**: 396–406.

25 **Takahashi, T., Dejbakhsh-Jones, S., and Strober, S.**, Expression of CD161 (NKR-P1A) defines subsets of CD4 and CD8 T cells with different functional activities. *J. Immunol.* 2006. **176**: 211–216.

26 **Annunziato, F., Cosmi, L., Santarlasci, V., Maggi, L., Liotta, F., Mazzinghi, B., Parente, E. et al.**, Phenotypic and functional features of human Th17 cells. *J. Exp. Med.* 2007. **204**: 1849–1861.

27 **Cosmi, L., De Palma, R., Santarlasci, V., Maggi, L., Capone, M., Frosali, F., Rodolico, G. et al.**, Human interleukin 17–producing cells originate from a CD161+CD4+ T cell precursor. *J. Exp. Med.* 2008. **205**: 1903–1916.

28 **Kleinschek, M. A., Boniface, K., Sadekova, S., Grein, J., Murphy, E. E., Turner, S. P., Raskin, L. et al.**, Circulating and gut-resident human Th17 cells express CD161 and promote intestinal inflammation. *J. Exp. Med.* 2009. **206**: 525–534.

29 **Maggi, L., Santarlasci, V., Capone, M., Peired, A., Frosali, F., Crome, S., Querci, V. et al.**, CD161 is a marker of all human IL-17-producing T-cell subsets and is induced by RORC. *Eur. J. Immunol.* 2010. **40**: 2174–2181.

30 **Tian, Y., Babor, M., Lane, J., Schulten, V., Patil, V. S., Seumois, G., Rosales, S. L. et al.**, Unique phenotypes and clonal expansions of human CD4 effector memory T cells re-expressing CD45RA. *Nat. Commun.* 2017. **8**: 1473.

31 **Sallusto, F., Geginat, J., Lanzavecchia, A.**, Central memory and effector memory T cell subsets: function, generation, and maintenance. *Annu. Rev. Immunol.* 2004. **22**: 745–763.

32 **Champagne, P., Ogg, G. S., King, A. S., Knabenhans, C., Ellefsen, K., Nobile, M., Appay, V. et al.**, Skewed maturation of memory HIV-specific CD8 T lymphocytes. *Nature* 2001. **410**: 106–111.

33 **Sallusto, F., Lenig, D., Förster, R., Lipp, M., and Lanzavecchia, A.**, Two subsets of memory T lymphocytes with distinct homing potentials and effector functions. *Nature* 1999. **401**: 708–712.

34 **Mittrücker, H., Visekruna, A., and Huber, M.**, Heterogeneity in the differentiation and function of CD8+ T cells. *Arch. Immunol. Ther. Exp. (Warsz)* 2014. **62**: 449–458.

35 **Mei, H. E., Leipold, M. D., and Maecker, H. T.**, Platinum-conjugated antibodies for application in mass cytometry. *Cytometry A* 2016. **89**: 292–300.

36 **Schulz, A. R., Baumgart, S., Schulze, J., Urbicht, M., Grützau, A., and Mei, H. E.**, Stabilizing antibody cocktails for mass cytometry. *Cytometry A* 2019. **95**: 910–916.

37 **Leipold, M. D., Newell, E. W., and Maecker, H. T.**, Multiparameter phenotyping of human PBMC using mass cytometry. *Methods Mol. Biol.* 2015. **1343**: 81–95.

38 **Chevrier, S., Crowell, H. L., Zaanotelli, V. R. T., Engler, S., Robinson, M. D., and Bodenmiller, B.**, Compensation of signal spillover in suspension and imaging mass cytometry. *Cell Syst.* 2018. **6**: 612–620.

39 **Budzinski, L., Schulz, A. R., Baumgart, S., Burns, T., Rose, T., Hirseland, H., and Mei, H. E.**, Osmium-labeled microspheres for bead-based assays in mass cytometry. *J. Immunol.* 2019. **202**: 3103–3112.

40 **Amir, E. D., Davis, K. L., Tadmor, M. D., Simonds, E. F., Levine, J. H., Bendall, S. C., Shenfeld, D. K. et al.**, viSNE enables visualization of high dimensional single-cell data and reveals phenotypic heterogeneity of leukemia. *Nat. Biotechnol.* 2013. **31**: 545–552.

41 **Chen, T. J., and Kotecha, N.** Cytobank: providing an analytics platform for community cytometry data analysis and collaboration. *Curr. Top. Microbiol. Immunol.* 2014. **377**: 127–157.

42 **Belkina, A. C., Ciccolella, C. O., Anno, R., Halpert, R., Spidlen, J., and Snyder-Cappione, J. E.**, Automated optimized parameters for T-distributed stochastic neighbor embedding improve visualization and analysis of large datasets. *Nat. Commun.* 2019. **10**: 5415.

Abbreviations: **AD**: Allergic donor · **CTL**: cytotoxic T lymphocyte · **DN**: double negative · **GZMB**: granzyme B · **HD**: Healthy donor · **HDM**: house dust mite · **MAIT**: mucosal associated invariant T · **MC**: mass cytometry

Full correspondence: Prof. Michael Lohoff, Institut für Medizinische Mikrobiologie und Krankenhaushygiene der Philipps Universität Marburg, Hans-Meerwein-Str. 2, 35043 Marburg, Germany
e-Mail: lohoff@med.uni-marburg.de

Received: 26/8/2020
Revised: 25/9/2020
Accepted: 19/11/2020
Accepted article online: 24/11/2020